DE-FG02-94ER45429-2

I. Progress During the Previous Funding Period

I-A. Status of the Small-Angle Diffractometer (SAND)

The SAND (Small Angle Neutron Diffractometer) instrument will be on the C3 beamline at IPNS, and is being built in three phases. Phase 1, a prototype, has been in place for more than a year and is being used to test components for the final instrument. This prototype includes one set of converging Soller collimators, the Ordela 40×40 cm^2 area detector, the Vaxstation 3520 computer, and most of the data acquisition electronics that are intended for the final instrument. Measurements on this prototype have so far concentrated on developments relating to the area detector, beam monitors, and shielding. Additional measurements are planned on collimators and on a chopper to remove delayed-neutrons and to eliminate frame-overlap. Positional resolution of 6 mm has been achieved on the area detector, and developments are underway to improve this to $\sim$4 mm. The chopper for eliminating delayed neutron background has been fabricated and will begin testing soon.

In Phase 2, the evacuated sample chamber and scattering chamber for the final instrument will be installed, along with their shielding. This flight path and sample chamber have been received, and IPNS personnel are in the process of installing the internal shielding in these pieces. Detailed design for the remainder of the components for this phase is nearly complete. The area detector will be mounted on this flight path, but the bank of linear-position-sensitive detectors (LPSDs) at higher scattering angles will not be installed at this time. A temporary mount for one set of converging Soller collimators will be installed in the incident beamline, and sufficient temporary shielding will be installed in the incident beamline, and the MgO crystals have been ordered for this filter. The delayed-neutron-removal chopper will probably be operated in the incident beamline as well. Operation in this mode will serve to shake down problems in the instrument and to characterize some aspects of the instrument performance, and should also permit some science. However, since the instrument will still be in a state of development and characterization, it will not be part of the User Program during this Phase.

In Phase 3, the final version of the incident beamline, including a well-engineered cooled MgO filter and an automated Soller-collimator changer will be installed. A second, tighter collimator will be installed in this changer along with the original collimator set. The changer will permit easy interchange of these two collimator sets, allowing the user to select the resolution necessary for the experiment. The bank of LPSDs will also be installed and the data acquisition electronics and software will be modified to operate with the combination of the area detector and LPSDs. This LPSD bank will use technology developed for the GLAD instrument at IPNS, and so will require little new development. This is expected to be the final version of the instrument, and once it is commissioned it will be available for the User Program. The attached figure shows the schematic layout of SAND in Phase 3.

SAND at IPNS

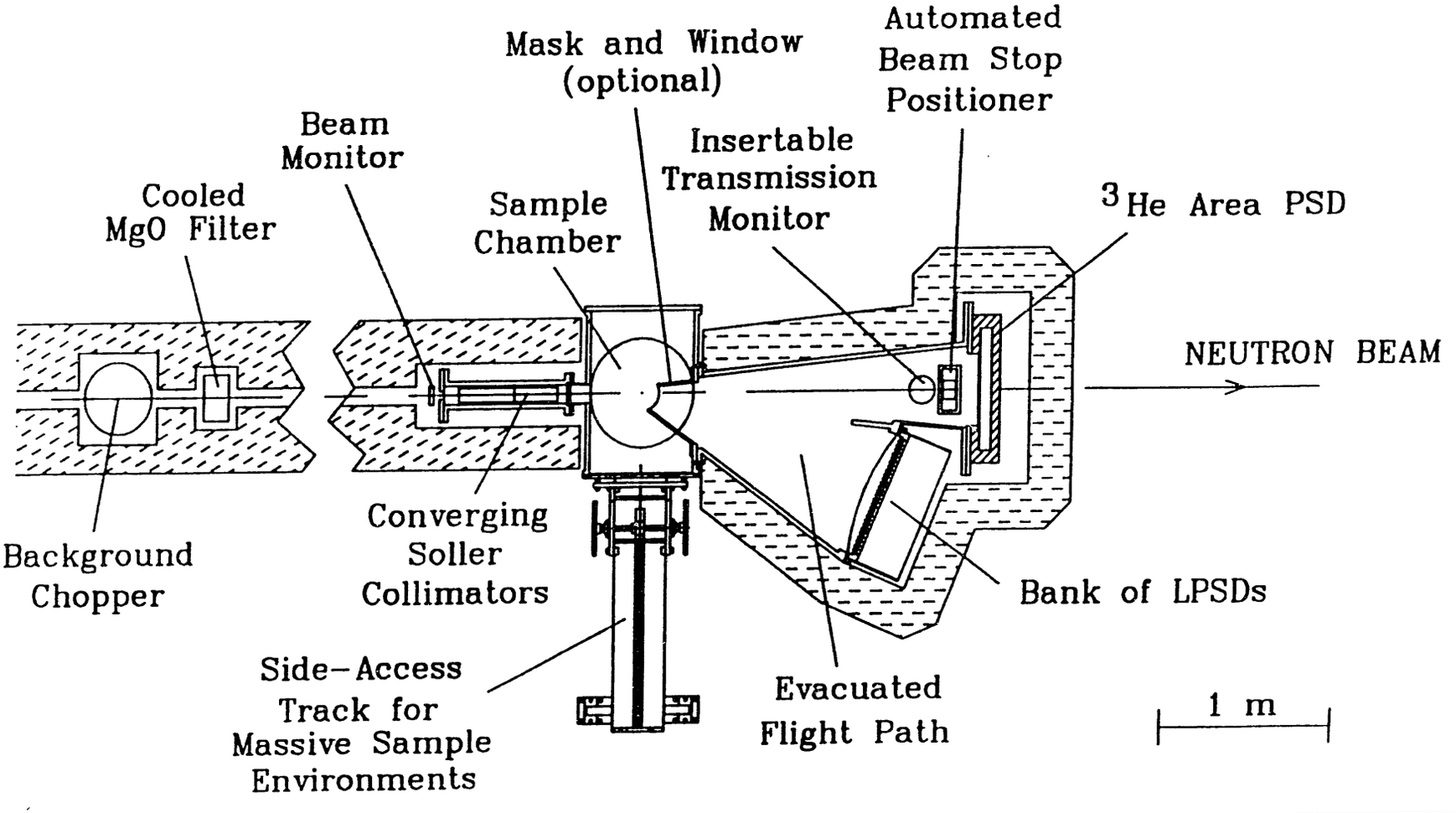

Figure 1

S A N D at I P N S

CHARACTERISTICS	Wide Q-range with fixed detectors
USE	Microemulsions, micellar solutions, dense colloid and polymer solution studies
WAVELENGTH RANGE	time of flight λ = 1 A - 14 A
FLUX AT THE SAMPLE	4 X 10^4 neutrons/cm^2sec
MODERATOR TO DETECTOR DISTANCE	9 meters
SAMPLE TO DETECTOR DISTANCE	2 meters
BEAM CONDITIONING DEVICES	delay neutron background chopper (a drum chopper); MgO filter (LN cooled); converging collimators FWHM 3 mr
SPECIAL SAMPLE ENVIRONMENT	window for observation of phase separation; good temperature control (0.01 ∘ K); shear cell; magnet
AREA DETECTOR	Ordela He^3 40 cm x 40 cm
AUXILIARY DETECTORS	linear position sensitive detectors 65 x 6 cm long
Q-RANGE	without LPSD 0.003 A^{-1} = 0.6 A^{-1} with LPSD 0.003 A^{-1} = 2.0 A^{-1}

I-A-1. Status of the sample environment equipment

In order to take advantage of the much wider range of scattering angles that will be available on SAND, new sample changers, furnaces, etc., are being provided. In the design of the sample environment we incorporate precision temperature control, see-through windows, and vertical sample positioning capability tailored for in situ phase separation studies.

I-A-2. Tentative schedule

Because of prior commitment of resources to the design and construction of the GLAD instrument at IPNS, the design and development of SAND has proceeded as a low priority item until roughly the last 15 months. Since that time, SAND has received much higher priority. The evacuated sample chamber and scattering flight path have now been received and shielding is being installed in this unit. MgO for the filter has been ordered. One set of collimators is in hand, as are the area detector and its complete set of data acquisition electronics and computer. Design of the remainder of the Phase 2 components should be completed by Spring, 1993. This design was scheduled for completion in Fall, 1992, but this schedule slipped once again due to the temporary shifting of resources to the development of the conceptual design for the IPNS-Upgrade project (a proposed 1 MW spallation neutron source at Argonne). If this design proceeds as currently scheduled, it should be possible to have the Phase 2 version of SAND installed on its beamline by the end of Summer, 1993, so that the commissioning of this instrument can begin in Fall, 1993. Completion of the Phase 3 instrument would be roughly one year later.

I-A-3. Funding

Total equipment expenditures on this instrument are roughly \$400 K to date. This does not include Argonne effort for design and construction, which has been significant. It is estimated that an additional ~\$100,000 will be required to complete Phase 2. A further ~\$300,000 will be required to complete Phase 3. With the exception of \$100,000 received from Texaco to date, this funding has been supplied by IPNS, and it is anticipated that IPNS will continue to supply most of the remaining required funding as well, to the extent that this is possible with its limited equipment budget. Roughly \$60,000 of the Texaco money has been used to buy the computer and some of the data acquisition electronics, to make some modifications to the area detector and its electronics, and to purchase some vacuum system components. The remainder of the Texaco money has not yet been committed.

In addition to this equipment funding, the first two years of the grant provided partial support for a post-doctoral student, Ken Bradley, who worked on some of the initial development efforts on the Phase 1 prototype, developed some of the requirements for the ancillary equipment, and contributed to the development of the data analysis software for SAND. These contributions were vital to the development of SAND.

I-B. 3–D Microstructure of Bicontinuous Microemulsions from SANS and Simulation

We previously performed SANS on a three-component ionic microemulsion system sodium di-2-ethylhexylsulfosuccinate (AOT)/D_2O/decane consisting of equal volume fractions of water and decane but with varying amounts of surfactant (volume fraction $0.181 < \phi_s < 0.420$) [1]. Near room temperature, we observed a prominent peak occurring at a finite wave vector transfer Q_{max} in the intensity distribution with Q_{max} increasing as ϕ_s according to the relation:

$$Q_{max} \approx \frac{2.25}{\Delta} \frac{\phi_s}{(1-\phi_s)^{2/3}} \tag{1}$$

where $\Delta = v_S/a_H$ is a molecular length given by the ratio of the steric volume of an AOT molecule, v_S, to the average area of an AOT molecule at the oil-water interface, a_H. This scaling relation can be derived from the conservation of surfactant volume and interfacial area, assuming that the microstructure of the microemulsion consists of closely packed spherical water droplets, each coated with a monolayer of AOT and dispersed in a continuum of decane. The origin of the scattering peak is therefore the inter-droplet correlation where the characteristic length scale is given by the average distance between two water droplets $d \approx \Delta(1-\phi_s)^{\frac{2}{3}}/\phi_s$.

This droplet phase forms because AOT at room temperature is more hydrophilic than lipophilic and visual evidence of this was later provided by freeze-fracture electron microscopy [2]. With a small amount of NaCl added to the water, the amphiphilicity of AOT becomes more balanced. When we studied AOT/D_2O(0.6% NaCl)/decane, we observed a similar peak in the SANS data. However in this case, the characteristic wave number Q_{max} varied according to the equation:

$$Q_{max} \approx \frac{0.5}{\Delta} \frac{\varphi_s}{\varphi_1 \varphi_2} \tag{2}$$

where $\varphi_1 = \phi_w + \alpha\phi_s$, $\phi_2 = \phi_o + (1-\alpha)\phi_s$, ϕ_w and ϕ_o are the volume fractions of D_2O and decane respectively, and $\alpha = 65/611$ is the ratio of the head group volume of AOT to the steric volume of the molecule. This second scaling relation is consistent with a bicontinuous structure as shown below.

The SANS intensity from a two-component porous medium can be written as [3]:

$$I(Q) = \langle\eta^2\rangle S(Q) = \langle\eta^2\rangle \int_0^\infty \Gamma(r) \frac{\sin(Qr)}{Qr} 4\pi r^2 \, dr \tag{3}$$

where $\langle\eta^2\rangle$ is the variance of the scattering length density. For our case, the first medium is water plus the head groups of AOT while the second is decane with the tails of AOT. $\Gamma(r)$, known as the Debye correlation function, is the normalized isotropic correlation function of spatial fluctuations in the scattering length density. Teubner and Strey [4] showed that for bicontinuous microemulsions with water-oil bulk contrast, the Debye correlation function

can be modelled as:

$$\Gamma_{TS}(r) = e^{-r/\xi}\frac{\sin(kr)}{kr} \tag{4}$$

where $d = 2\pi/k$ is the average distance between water-water or oil-oil domains and ξ is the coherence length of this short range order. $\Gamma_{TS}(r)$, when substituted into Eq. (3), gives rise to a peak at $Q_{max} = \sqrt{k^2 - 1/\xi^2}$. Also, the slope of $\Gamma_{TS}(r)$ at $r = 0$ is related to the interfacial area per unit volume S/V, by $\Gamma'_{TS}(0) = -1/\xi = -(S/V)/(4\phi_1\phi_2)$ [3]. For a monolayer of AOT between the water and oil domains, $S/V = \phi_s/\Delta$. From these relations, we get:

$$Q_{max} = \frac{\sqrt{k^2\xi^2 - 1}}{4\Delta}\frac{\phi_s}{\phi_1\phi_2} \tag{5}$$

In order to identify Eq. (5) with Eq. (2), we must have $k\xi = 2.24$. Our SANS experiments indicate that for $0.10 < \phi_s < 0.25$, $k\xi$ lies in the range $\pi/2 < k\xi < \pi$ [5]. As the temperature is varied at constant ϕ_s, the phase diagram of AOT/D_2O(0.6% NaCl)/decane evolves from a two-phase coexistence (water-in-oil microemulsion and water) into a bicontinuous one-phase region and then into another two-phase coexistence (oil-in-water microemulsion and oil). This structural evolution was studied by SANS [6] and it was found that $k\xi$ may be interpreted as a disorder parameter which is minimized when the hydrophilicity and lipophilicity of AOT becomes exactly balanced. At this temperature, $T = 41°C$, the spontaneous curvature of the AOT monolayer is zero and curves neither towards water nor towards oil.

To visualize this interesting microstructure, we use a simulation scheme first proposed by Berk [7]. Assuming that the microemulsion may be adequately represented by clipping a Gaussian random variable $\Psi(\vec{r})$, whose spectral distribution is of the form:

$$f(Q) = \langle|\Psi(Q)|^2\rangle = \frac{(b/\pi^2)[a^2 + (b+c)^2]}{(Q^2 + c^2)[Q^4 + 2(b^2 - a^2)Q^2 + (a^2 + b^2)^2]} \tag{6}$$

From this expression, the correlation of the Gaussian random field given by the expression $g(r) = \langle\Psi(0)\Psi(r)\rangle = \int_0^\infty f(Q)\sin(Qr)/(Qr)\,4\pi Q^2\,dQ$ may be calculated analytically. Berk showed that $g(r)$ is related to the Debye correlation function for the oil-water bulk contrast by $\Gamma_B(r) = \frac{2}{\pi}\sin^{-1} g(r)$ [7].

We may also calculate the Debye correlation function for scattering with film contrast (deuterating both oil and water) from $g(r)$. For a thin surfactant layer, we derive the result:

$$\Gamma_S(r) = \frac{\frac{1}{\sqrt{1-(1-\phi_s^2)^2 g(r)^2}} - 1}{\frac{1}{\sqrt{2-\phi_s^2}} - \phi_s}\,\phi_s. \tag{7}$$

Fig. 2 and Fig. 3 show the normalized experimental (circles) and calculated (solid line) scattering curves for bulk and interface contrast respectively. The parameters used to obtain these fits are $a = 0.0172\text{Å}^{-1}$, $b = .00976\text{Å}^{-1}$, and $c = .0417\text{Å}^{-1}$.

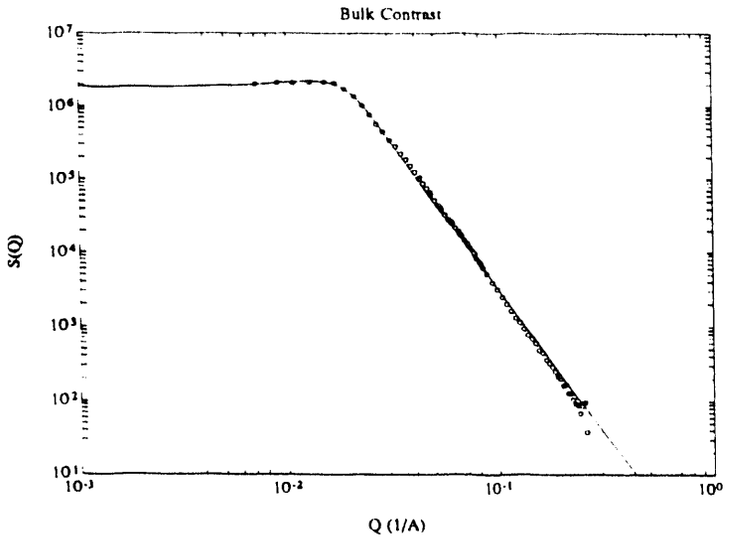

Figure 2: Bulk scattering of AOT/D_2O(0.6% NaCl)/decane with $\phi_s = 0.10$ at $T = 41°C$. Experimental data is shown with circles and the calculated solid line was obtained with $a = 0.0172\text{Å}^{-1}$, $b = .00976\text{Å}^{-1}$, and $c = .0417\text{Å}^{-1}$.

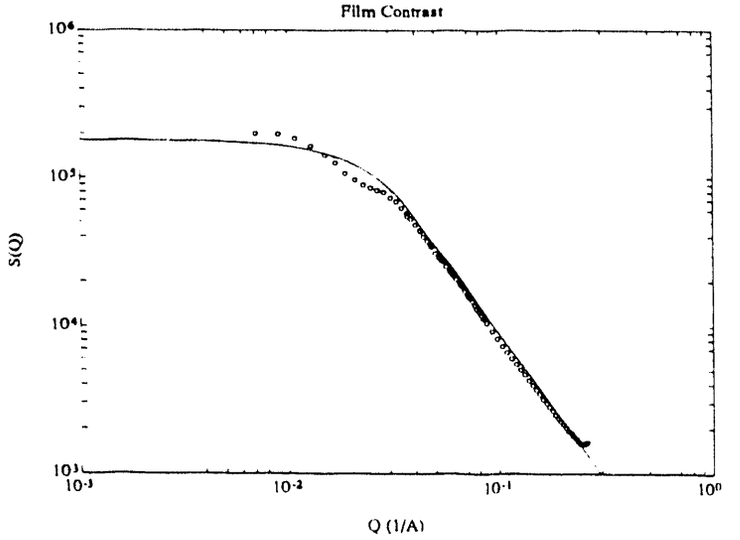

Figure 3: Film scattering of AOT/D_2O(0.6% NaCl)/decane with $\phi_s = 0.10$ at $T = 41°C$. Experimental data is shown with circles and the calculated solid line was obtained with the same parameters as in Fig. (2).

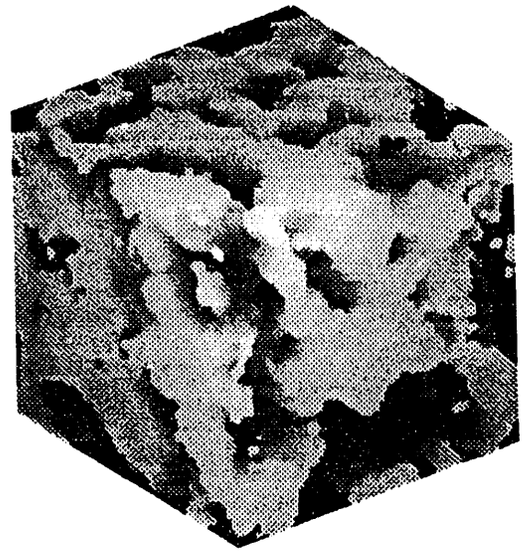

Figure 4: Generated real space microstructure using 10,000 random cosine waves.

The simulated real space microstructure is then obtained by summing very many (10,000) cosine waves having a spectral distribution given by Eq. (6) with the above parameters and random phases. A perspective view of such a generated structure is shown in Fig. 4.

From the form of Eq. (6), we can identify the parameters a and b with the equivalent parameters k and $1/\xi$ in the Teubner-Strey model. However, the parameter c is new in that it acts as a Q^{-6} cut-off frequency for the spectral distribution and is related to a microscopic cut-off length scale on the order of the inter-surfactant distance where the continuum model is no longer valid.

I-C. Local Geometry of the Surfactant Monolayer in Microemulsions

In a bicontinuous microemulsion, the monolayer sheet of surfactant separating oil and water domains can be visualized as a random, isotropic, self-avoiding, two-dimensional surface undergoing thermal fluctuations. Such random surfaces are of particular interest for statistical physics and it would be useful if direct experimental measurements could be made of the topology and local geometry of these model systems.

We propose to employ small-angle neutron scattering (SANS) along with hydrogen-deuterium contrast variation to determine quantitative geometrical characteristics of the surfactant sheet. In particular, we feel that it is possible to measure the mean and Gaussian curvatures of the monolayer. At any point on the surfactant surface, two principal radii of curvature can be found (Fig. 5). The mean curvature with respect to the water phase is

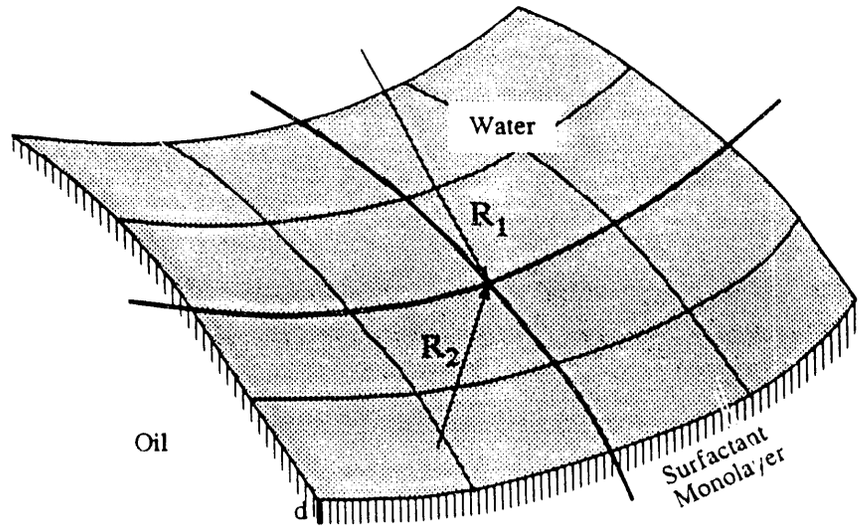

Figure 5: Schematic showing local curvatures at a point on the surfactant monolayer.

defined as the statistical average $\langle 1/R_1 \rangle$ and the Gaussian curvature is given by $\langle 1/R_1 R_2 \rangle$. Generally in the past, SANS has mainly been used as a tool to determine sizes of mesoscopic objects, e.g. radii of gyration, layer spacings, inter-particle distances, etc. We can show how, by using isotopic contrast and high-quality SANS measurements of different interfacial areas, it is possible to determine information about the curvature of a surface.

What makes the measurement of these curvatures so important? As mentioned above, the amphiphilicity of a surfactant can vary tremendously depending upon external conditions. The most obvious manifestation of this change is the mean curvature as the surfactant sheet bends preferentially towards either the water or oil domains. A careful measurement of this curvature will yield information about the hydrogen bonding and van der Waals interactions between the surfactant, water, and oil molecules. On the other hand, the Gaussian curvature is particularly interesting because it connects the local geometry of the surface with the global topology of the phase through the Gauss-Bonnet theorem. Measuring the Gaussian curvature will give the number of topological "handles" of the surface. It has been proposed that the energy contribution associated with the Gaussian curvature is the driving force behind the microemulsion assuming a bicontinuous, spherical, or lamellar structure. Others have claimed that the energy contribution of the mean-squared curvature term is more important. A careful experimental measurement will be useful in resolving this controversy.

Due to the chain length of the surfactant, the monolayer sheet will have a finite thickness. The water-surfactant interfacial area and the oil-surfactant interfacial area need not be the same and in fact, will be equal only when the mean curvature of the surfactant film vanishes. Thus, accurate measurements of the two interfacial areas can lead to the determination of the mean curvature of the monolayer. In order to obtain the Gaussian curvature of the monolayer, another measurement of the surface area at the midpoints of the surfactant

molecules is needed. These three areas are geometrically related by the following equations:

$$A_{WS} = A_S \left(1 - d\left\langle \frac{1}{R_1} \right\rangle + \frac{d^2}{4}\left\langle \frac{1}{R_1 R_2} \right\rangle\right) \tag{8}$$

$$A_{OS} = A_S \left(1 + d\left\langle \frac{1}{R_1} \right\rangle + \frac{d^2}{4}\left\langle \frac{1}{R_1 R_2} \right\rangle\right) \tag{9}$$

where A_{WS} and A_{OS} are the water-surfactant and oil-surfactant interfacial areas respectively and A_S is the surface area of the monolayer film at the center of the surfactant molecules.

Using hydrogen-deuterium isotopic substitution in both the water and oils, we can highlight and isolate the various interfacial and surfactant surfaces in a SANS experiment. From the form of the resulting scattering at intermediate to large wave vector transfers, we can then obtain the different areas using Porod's relation.

From the above equations, we see that mean curvature modifies A_{WS} and A_{OS} to first order while the Gaussian curvature comes in as a second order term. This makes measuring the mean curvature relatively easy and determining the Gaussian curvature technically more difficult. A typical value for $d/R \approx (20\text{Å})/(100\text{Å})$ means that we need to determine the three areas to less than 1% error. Such accuracy implies that long counting times be used and very careful analysis of the resulting data be performed. To this end, we have already developed most of the software enabling us to reduce multiple two-dimensional data sets, correct for resolution effects and multiple-scattering, and precisely fit the resulting scattering patterns while maintaining good estimates on the associated errors. With the current growth of SANS, it is anticipated that these programs will also be useful to a number of users at these facilities.

We have already performed some preliminary studies using the H9B spectrometer at Brookhaven National Laboratory and the 30m NSF SANS instrument at the National Institute of Standards and Technology. The system used is water/octane/tetraethylene glycol monodecyl ether ($C_{10}E_4$) and its phase diagram is shown in Fig. 6. The data for three different contrasts of the microemulsion is shown in Fig. 7 which show the characteristic decay of scattering from the two interfaces and the surfactant film. The values of the surface to volume ratios we got from the analysis which are shown by the solid line fits in Fig. 7 are: $A_{ws} = (6.05 \pm .03) \times 10^{-3}\,\text{Å}^{-1}$, $A_{os} = (5.95 \pm .03) \times 10^{-3}\,\text{Å}^{-1}$ and A_s is less certain. From these values and Eq (8) and (9) we deduced the mean curvature as $\langle 1/R \rangle = (-5 \pm 3) \cdot 10^{-4}\,\text{Å}^{-1}$. This near-zero mean curvature is consistent with the symmetric location in the phase diagram of the phase point studied. However, determination of the Gaussian curvature is indeed technically more challenging. In particular, we have discovered significant oil and water penetration into the monolayer which decreases the contrast between the surfactant film and the other phases and affects the measurement of A_S. However, we feel that this difficulty can be overcome by further studies and carefully measuring the scattering over a wide range of wave vector transfers. Then determination of the invariant, an integration of the scattering pattern, will yield another measured quantity which will enable us to accurately determine the monolayer surface area and hence the Gaussian curvature.

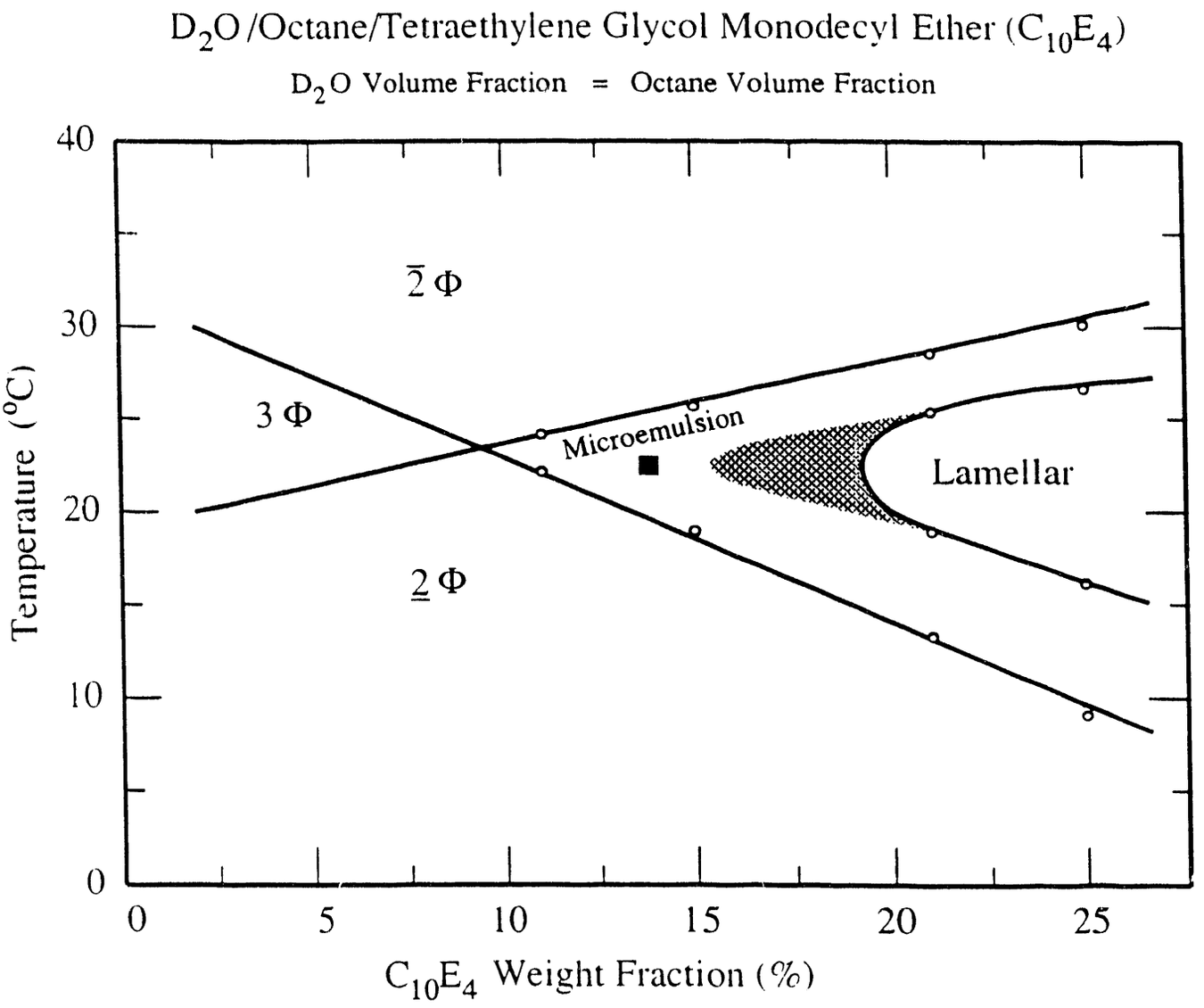

Figure 6: Phase Diagram for D_2O-Octane-$C_{10}E_4$. The phase point used in this study is marked with a square.

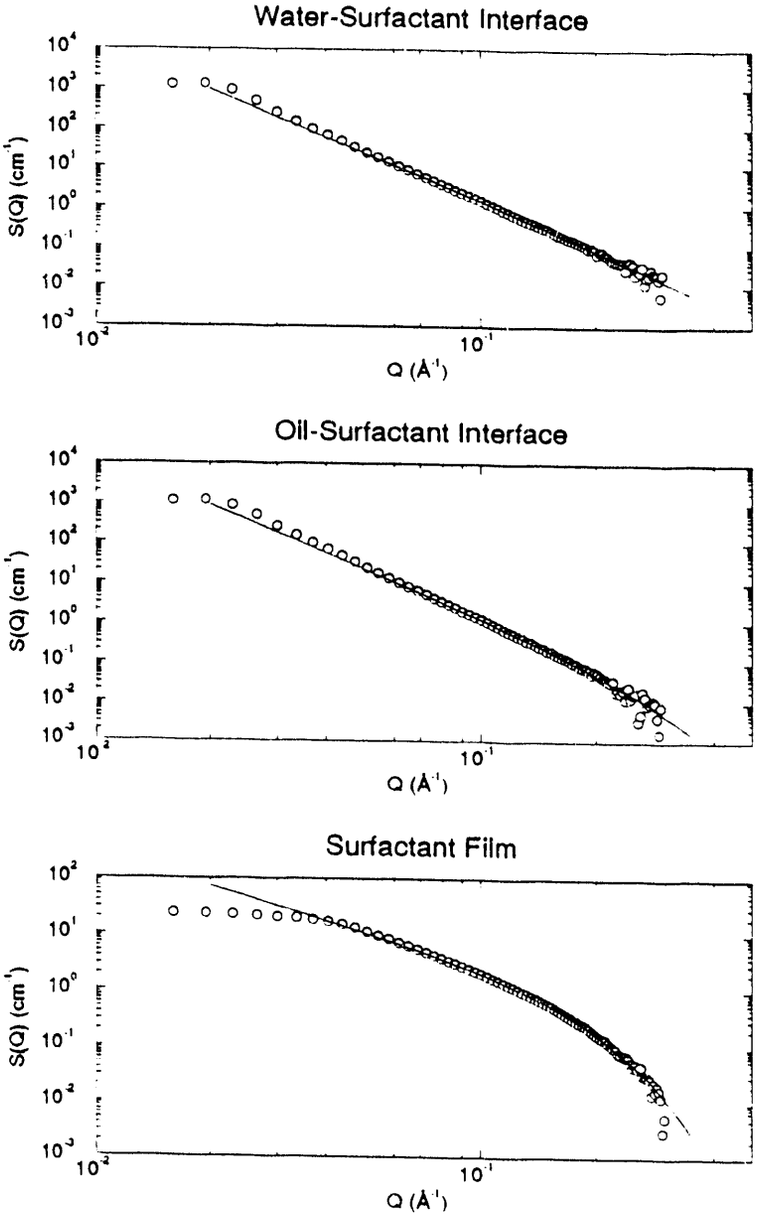

Figure 7: SANS from the microemulsion with different contrasts.

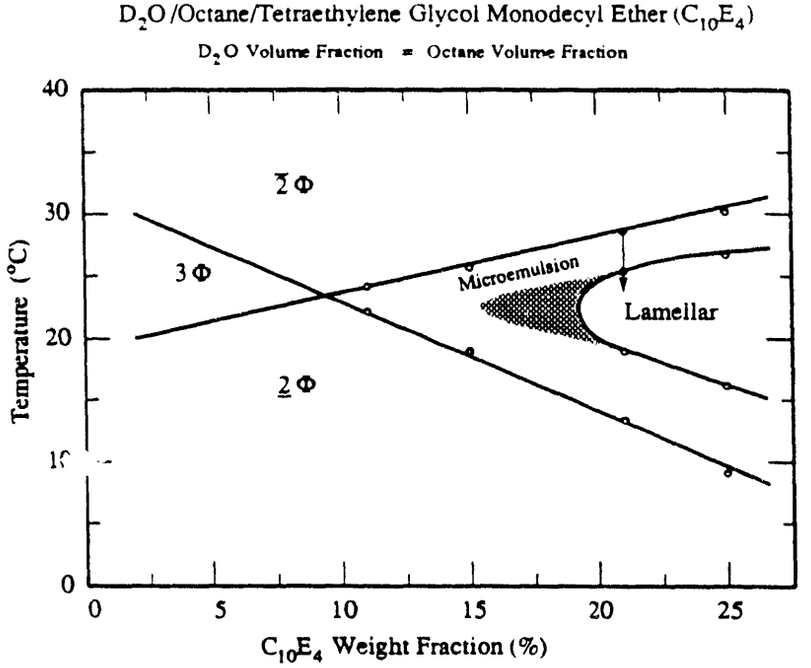

Figure 8: The phase trajectory used in this study is indicated by the arrow in the phase diagram.

With further study and analysis, determination of both mean and Gaussian curvatures of a surfactant monolayer should be possible using SANS and contrast variation. In conjunction with our other work, these curvature measurements will be valuable for a better understanding of the chemical interactions in and physical fluctuations of these films.

I-D. Surface Ordering in Microemulsions

Bicontinuous microemulsions are isotropic and exhibit complete rotational invariance. In contrast, lamellar phases spontaneously break this symmetry and their sheet normals prefer a certain spatial orientation. These phases are typically situated adjacent to each other on a phase diagram with a first-order transition separating the two. We have started to investigate the effect of surfaces on ordering the bulk, isotropic bicontinuous phase near this transition using neutron reflectivity.

Presumably near the lamellar transition, fluctuations of monolayers aligning in parallel planes will become more and more dominant. The presence of a surface could cause this effect to become more pronounced and can be detected using specular reflectivity off these surfaces. Fig. 8 and Fig. 9 show the phase diagram and some preliminary data of a microemulsion near the lamellar transition that we have recently taken using the BT7 Grazing-Angle Spectrometer at the National Institute of Standards and Technology. The

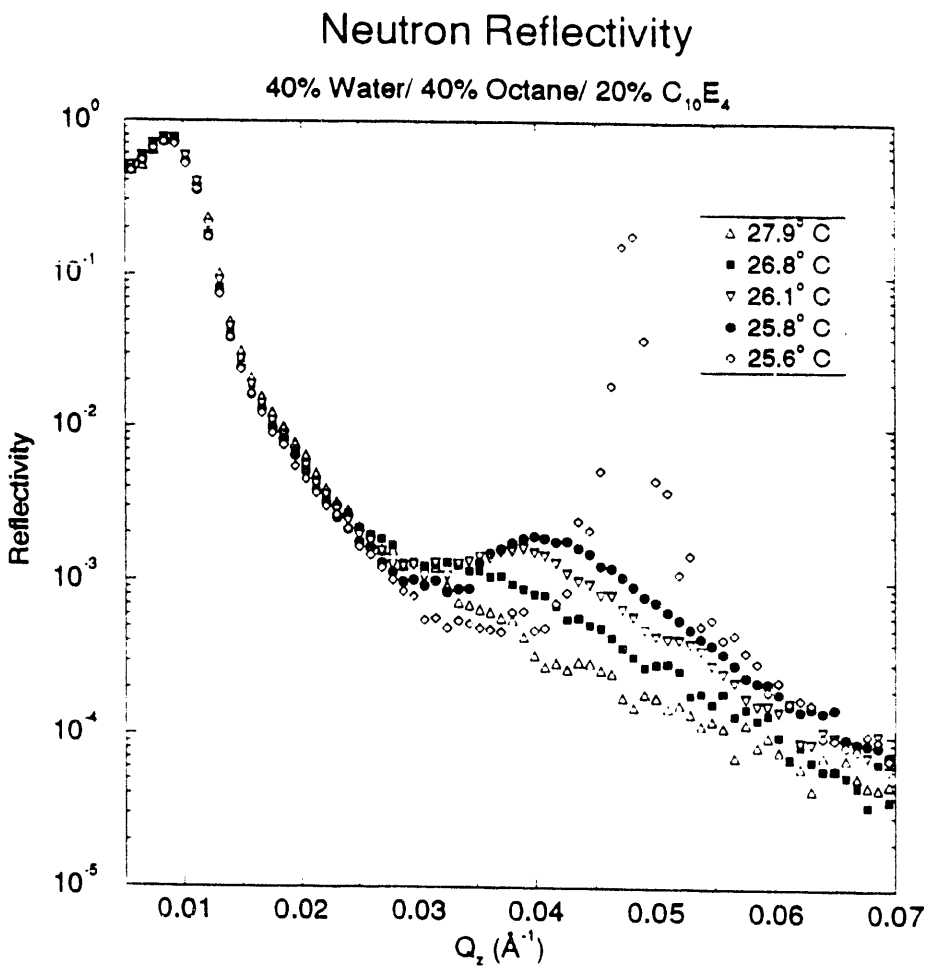

Figure 9: Effect of temperature on the surface ordering of a microemulsion near the lamellar transition.

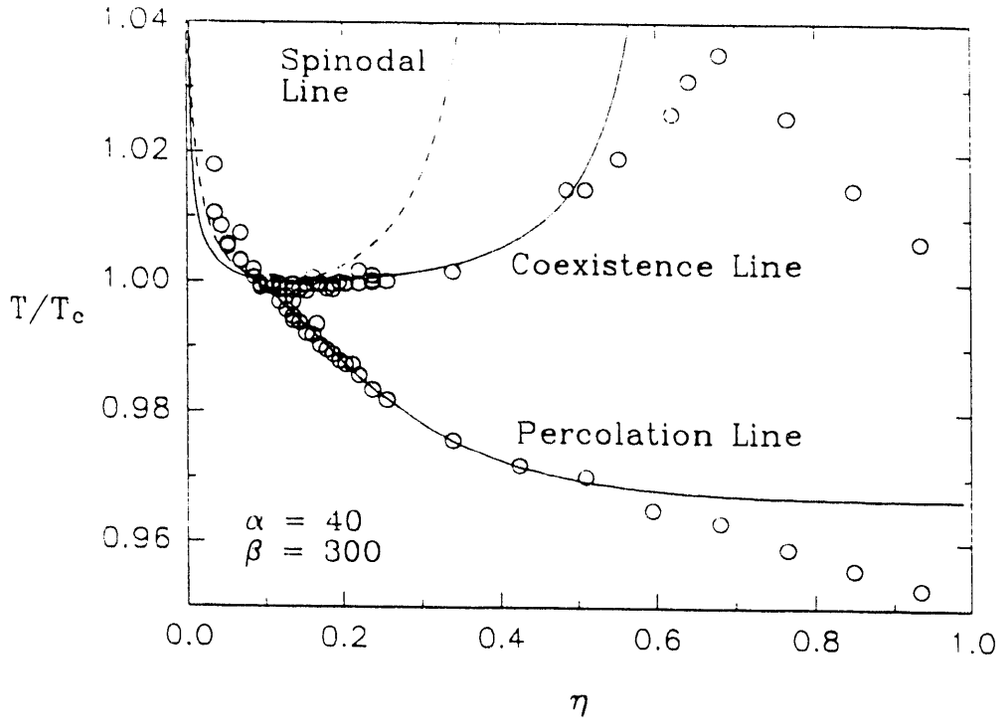

Figure 10: Phase diagram of the AOT/water/decane microemulsion system. Solid lines are the sticky sphere model.

microemulsion consisted of water, octane, and tetraethylene glycol monodecyl ether ($C_{10}E_4$) near a silicon surface treated to make it hydrophobic.

As can be seen, as the temperature approached the lamellar transition, the effect of surface ordering becomes very pronounced as a broad bump in the reflectivity profile. The sharp peak at the last temperature shows exactly when the lamellar region is reached. We are still in the process of interpreting this data and are contemplating further studies where we will be able to relate the bulk structural information from SANS with surface-specific information obtained from reflectivity.

I-E. Dynamics of Water-in-oil Droplet Microemulsions

The three-component ionic microemulsion system consisting of AOT/water/decane shows an interesting phase behavior in the vicinity of room temperature. The phase diagram in the temperature-volume fraction (of the dispersed phase) plane exhibits a lower consolute critical point around 10% volume fraction and a percolation line, cutting across the plane starting from the vicinity of the critical point, extends to high volume fraction side at progressively lower temperatures. This phase behavior can be understood in terms of a system of polydispersed spherical water droplets, each coated by a monolayer of AOT, dispersed in a continuum of oil. These droplets interact with each other via hard-core plus a short-range

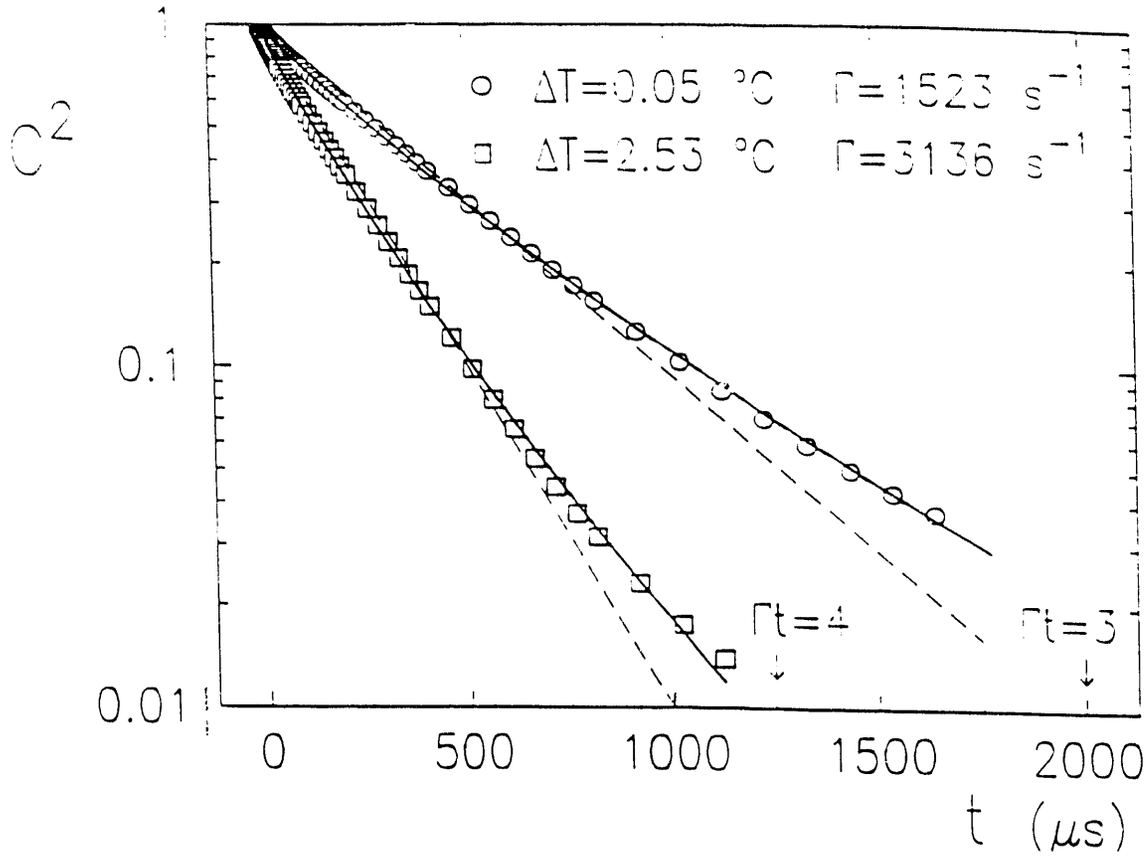

Figure 11: Measured squared photon correlation function showing deviation from the exponential behavior in a AOT/water/decane droplet microemulsion system.

attractive interaction, the strength of which increases with temperature. We show that Baxter's sticky sphere model can quantitatively account for the phase behavior including the percolation line, provided that the stickiness parameter is a suitable function of temperature (Fig. 10). We use the structure factors measured by small-angle neutron scattering below the critical temperature to determine this functional dependence. We also investigate the dynamics of droplets below and approaching the percolation line by dynamic light scattering. Both the first cumulant and the droplet density time correlation function can be quantitatively calculated by assuming the existence of polydispersed fractal clusters formed by the microemulsion droplets due to the attraction. Analysis of SANS data indicates that above the percolation line, the clustered droplets structure gradually transforms into an ordered bicontinuous structure [8].

We also made precise measurements of the droplet-density time correlation function in a pseudo two-component water-in-oil microemulsion system, made of AOT-coated water droplets dispersed in decane, close to its consolute critical pint. Systematic studies of the intensity correlation functions using a correlator with a logarithmic sampling time show sizeable deviations from a single exponential delay (Fig. 11). An extension of the dynamic droplet model is able to account for the non-exponential behavior at intermediate and long

times. The linewidth we obtain is in satisfactory agreement with the model, which takes into account the finite size of the microemulsion droplets [9].

I-F. Micellar Formation and Correlation in the Cavity of Porous Silica Glass

We are using SANS to study length-density correlations in a dry, porous silica glass (Vycor) and in a glass filled with anionic and cationic surfactant molecules dispersed in water [10]. SANS intensity distributions from empty pores of the glass can be satisfactorily analyzed using a standard late-stage spinodal decomposition model in which the porous structure (the glass) is described by a superposition of random density waves. This model, however, agrees with experiment only if one allows for a suitable distribution of wave numbers for the density waves. We have observed micellar formation in Vycor filled with surfactant solution. We interpreted the intermicellar correlations, measured by SANS, within the surfactant solution and within the pores of the Vycor glass. As a next step, we shall study phase transitions and microstructure of bicontinuous one-phase non-ionic three-component microemulsions in the cavities of Vycor glass.

References

[1] M. Kotlarchyk, S. H. Chen, J. S. Huang, M. W. Kim. *Phys. Rev. Lett.* **53**, (1984).

[2] W. Jahn and R. Strey. *J. Phys. Chem.* **92**, 2294, (1988).

[3] P. Debye, H. R. Anderson, Jr., and H. Brumberger. *J. Appl. Phys.* **28**, 679, (1957).

[4] M. Teubner and R. Strey. *J. Chem. Phys.* **87**, 3195, (1987).

[5] S. H. Chen, S. L. Chang, R. Strey. *J. Appl. Cryst.* **24**, 721, (1991).

[6] S. H. Chen, S. L. Chang, R. Strey, J. Samseth, K. Mortensen. *J. Phys. Chem.* **95**, 7427, (1991).

[7] N. F. Berk. *Phys. Rev. Lett.* **58**, 2718, (1987).

[8] S. H. Chen, C. Y. Ku, J. Rouch, P. Tartaglia, C. Cametti, J. Samseth, to appear in *J. de Physique.*

[9] J. Rouch, P. Tartaglia, S. H. Chen, submitted to *Phys. Rev. Lett.*

[10] K. F. Bradley, S. H. Chen, P. Thiyagarajan, *Phys. Rev.* **A42**, 6015, (1990).

I-G. Project Output

I-G-1. Major recent accomplishments

For the past three years, we have focused our attention on understanding the phase-behavior and microstructure relationship in microemulsions, especially in the region of the phase diagram where the structure is thought to be bicontinuous. We have used SANS and simulation methods to visualize the 3-D morphology in these systems. Also using SANS, we investigated the structural inversion from a water-in-oil to an oil-in-water microemulsion through the bicontinuous regime. We also studied static and dynamic critical phenomena of micellar systems and in droplet microemulsions and the dynamical theory of critical phenomena was extended to the percolation transition in water-in-oil droplet microemulsions. We also analyzed the correlations in micellization by ionic surfactants in porous Vycor glass.

I-G-2. Bibliography of publications emanating from this project

1. K. F. Bradley, S. H. Chen, P. Thiyagarajan. "Micellar Formation and Correlation in the Cavity of Porous Silica Glass," *Phys. Rev.* **A42**, 6015–6023, 1990.

2. S. H. Chen, S. L. Chang, R. Strey, J. Samseth, K. Mortensen. "Structural Evolution of Bicontinuous Microemulsions," *J. Phys. Chem.* **95**, 7427–7432, 1991.

3. S. H. Chen, S. L. Chang, R. Strey, P. Thiyagarajan. "Small Angle Neutron Scattering Investigation of Structural Inversion in a Three-Component Microemulsion," *J. Phys. Condensed Matter* **3**, F91-F107 (1991), invited to "International Symposium on the Structure and Dynamics of Liquids and Gases," Wadham College, Oxford University, April 1991.

4. S. H. Chen, S. L. Chang, R. Strey, P. Thiyagarajan. "Investigation of the Temperature Induced $L3 - L - L1$ Structural Transitions within the One-Phase Channel of a Three-Component Microemulsion by Small Angle Scattering," invited to "Structure and Conformation of Amphiphilic Membranes," Julich, Germany, September, 1991, published in *The Structure and Conformation of Amphiphilic Membranes*, eds. R. Lipowsky, D. Richter, K. Kremer. Springer-Verlag, p. 281–286, 1992.

5. S. H. Chen and S. L. Chang. "Theory of Scattering from Bicontinuous Structures," *Structure and Dynamics of Strongly Interacting Colloids and Supramolecular Aggregates in Solution*, eds. S.H. Chen, J.S. Huang, P. Tartaglia, NATO ASI Series, C, **369**, p. 659-690, 1992.

6. S. H. Chen, J. Rouch, P. Tartaglia. "Dynamic Slowing-Down in Dense Microemulsions Near the Percolation Threshold," invited paper "International Symposium on Slow Dynamics in Condensed Matter," Fukuoka, Japan, Nov. 1991, published in *AIP Conference Proceeding 256*, eds. K. Kawasaki, M. Tokuyama and T. Kawakatsu, p. 301-317, 1992.

7. S. H. Chen, D. Lee, S. L. Chang. "Visualization of 3-D Microstructure of Bicontinuous Microemulsions by Combined SANS Experiments and Simulations," invited to European Physical Society, Liquid State Conference: "Neutron Scattering From Liquid Matter," Gianini Naxos, Italy, Sept. 1992, to be published *J. Mol. Structure* (U.K.), 1993.

8. X. L. Zhou, L. T. Lee, S. H. Chen, R. Strey. "Observations of Surface-Induced Layering in Bicontinuous Microemulsions," *Phys. Rev.* **A46**, 6479-6489, 1992.

9. S. H. Chen, C. Y. Ku, J. Rouch, J. Samseth, P. Tartaglia, C. Cametti. "Structure and Dynamics of Dense Water-in-Oil Microemulsions Below and Above the Percolation," invited to "Complex Liquid Systems," Calabria, Italy, July 1992, to be published *J. de Physique*, 1993.

10. X. L. Zhou and S. H. Chen. "A Model-Independent Method for Reconstruction of Scattering-Length Density Profiles using Neutron or X-ray Reflectivity Data," to be published *Phys. Rev.* **E**, May 1993.

11. S. H. Chen, X. L. Zhou, B. L. Carvalho. "Inverse Problems in Neutron and X-ray Reflectivity Studies," a plenary lecture to the Annual European Colloid and Interface Science Society, Graz, Austria, Sept. 1992, to be published in *Progr. Colloid and Polymer Science*, 1993.

12. A. DiBiasio, C. Cametti, P. Codastefano, P. Tartaglia, J. Rouch, S. H. Chen. "Phase Behavior of Dense Three-Component Ionic Microemulsions and Electrical Conductivity," to be published *Phys. Rev.* **E**, 1993.

13. P. LoNostro and S. H. Chen. "Aggregation of a Semifluorinated n-Alkane in Perfluorooctane," to be published *J. Phys. Chem.*, 1993.

14. J. Rouch, P Tartaglia, S. H. Chen. "Experimental Evidence of Non-Exponential Relaxation Near the Critical Point of a Supramolecular Liquid Mixture," submitted to *Phys. Rev. Lett.*, March 1993.

15. B. L. Carvalho, P. Tong, J. S. Huang, T. A. Witten, L. J. Fetters. "Adsorption of End-Functionalized Polymers on Colloidal Spheres," to be published in *Macromolecules*, 1993.

16. B. L. Carvalho and S. H. Chen. "A Low-Wave Vector Expansion for Reflectivity," *Phys. Rev.* **E47**, 743-746, 1993.

17. S. L. Chang, C. Y. Ku, S. H. Chen, J. S. Lin. "Measurement and Interpretation of Counterion Distributions Around Cylindrical Micelles" invited to the 9th International Conference on Small Angle Scattering, Saclay, France, April 1993, to be published in *J. de Physique*.

18. P. Baglioni, Y. C. Liu, S. H. Chen, J. Teixeira, "Structure and Aggregation of Lithium Dodecylsulfate Micellar Solution in the Presence of a Macrocylic Cage: A SANS Study," presented at the 9th International Conference on SAS, Saclay, France, April 1993, to be published in *J. de Physique*.

19. D. D. Lee, J. Barker, S. H. Chen, "Absolute Calibration of Small Angle Neutron Scattering Data using Strong Coherent Scattering," presented at the 9th International Conference on SAS, Saclay, France, April 1993, to be published in *J. de Physique*.

20. B. L. Carvalho, S. H. Chen, W. D. Dozier, G. P. Felcher, "Interlayer Diffusion in a Langmuir-Blodgett Film as Revealed by Neutron Reflectivity," submitted to *Langmuir*, 1993.

BOOK

1. S. H. Chen, J. S. Huang, P. Tartaglia, editors. *Structure and Dynamics of Strongly Interacting Colloids and Supramolecular Aggregates in Solution*, NATO ASI Series C **369** (1992).

abstract retained ds

END

DATE FILMED

11/29/93